京都大学学術情報リポジトリ
KURENAI 紅
Kyoto University Research Information Repository

京都大学
KYOTO UNIVERSITY

Title	Field-ionization processes in high Rydberg states of Rb under a rotating electric field
Author(s)	Yamada, S; Funahashi, H; Shibata, M; Kominato, K; Kishimoto, Y; Tada, M; Haseyama, T; Ogawa, I; Matsuki, S; Yamamoto, K
Citation	PHYSICAL REVIEW A (2005), 72(3)
Issue Date	2005-09
URL	http://hdl.handle.net/2433/39831
Right	Copyright 2005 American Physical Society
Type	Journal Article
Textversion	none; publisher

Kyoto University

Field-ionization processes in high Rydberg states of Rb under a rotating electric field

S. Yamada* and H. Funahashi
Department of Physics, Kyoto University, Kita-Shirakawa, Sakyo-ku, Kyoto 606-8503, Japan

M. Shibata, K. Kominato, Y. Kishimoto, M. Tada, T. Haseyama, I. Ogawa,† and S. Matsuki
Nuclear Science Division, Institute for Chemical Research, Kyoto University, Gokasho, Uji, Kyoto 611-0011, Japan

K. Yamamoto
Department of Nuclear Engineering, Kyoto University, Yoshida, Sakyo, Kyoto 606-8501, Japan
(Received 2 December 2004; published 20 September 2005)

Field ionization of high Rydberg manifold states ($n=112$–137) of rubidium-85 under a rotating electric field has been investigated experimentally and theoretically. Applying a rapidly reversed electric field with a small static perpendicular field to rotate the total electric field around zero, we have observed substantial increase of the fraction of the tunneling field-ionization process and a profound broadening of its ionization peak over a wide range of field strengths with increasing transverse electric field. The observed tunneling field-ionization fraction is almost independent of the slew rate of the applied electric field, and also on the principal quantum number n over the range investigated. To compare with these experimental results, theoretical calculations have been performed with a successive two-step regime. As the first step we calculated the redistributions of magnetic quantum number m_ℓ and parabolic quantum number n_1-n_2 of the states under the rotating electric field. Then the following time evolution of the manifold states with $|m_\ell|\leqslant 3$ was traced on the Stark map in a coherent as well as an incoherent model. The calculated results are generally in good agreement with the experimental ones. The increase of the tunneling field-ionization fraction under a rotating electric field plays an essential role in achieving the high efficiency in the recently proposed selective-field-ionization scheme for high Rydberg atoms.

DOI: 10.1103/PhysRevA.72.033414 PACS number(s): 32.80.Rm, 32.60.+i, 79.70.+q

I. INTRODUCTION

In the nonhydrogenic atoms, there occur generally two field-ionization processes [1–5]. One is the tunneling process, where a valence electron escapes through tunneling from the barrier produced by the Coulomb potential plus the externally applied electric field. The ionization threshold value for this process is higher for higher excited states in the manifold (linear Stark states of the same n), in which the lowest manifold state is ionized at the classical saddle-point value. The other process is an autoionizationlike process, which occurs through level mixing in the ionic core and thus through the transition of the hydrogenically bound state to continuum states with lower parabolic quantum number n_1 and higher principal quantum number n. In this process the ionization threshold field is quite near to the classical saddle point value and thus lower than the value from the hydrogenic tunneling process.

Which of the two processes does actually occur depends on the coupling strength between the bound state and the continuum states of higher n. Taking into account the coupling strength above, the ionization rate Γ_{auto} through the autoionizationlike process is roughly given by

$$\Gamma_{\text{auto}} \sim \pi \frac{\sin^2 \delta'_\ell}{n^4}, \tag{1}$$

where δ'_ℓ is the magnitude of the difference between the quantum defect δ_ℓ and the nearest integer [4]. The ionization rate of low-m_ℓ states through the autoionizationlike process is thus generally higher than of high-m_ℓ states, because the low-ℓ states have large quantum defects. Rydberg states are usually populated by laser excitations from low-lying states near the ground state. Therefore they are allowed to have only $|m_\ell|$ close to zero due to the selection rule. In this case, the autoionizationlike process usually dominates in the ionization.

However it is possible to alter this situation by applying a rotating electric field during the course of time evolution in a Stark map: When the direction of the external electric field is rotated, the cylindrical symmetry and thus the conservation of $|m_\ell|$ values along the initial axis of the electric field are broken; thereby appreciable change may occur in the m_ℓ distributions.

The main purpose of the present work is to study the effect of the rotating electric field on the field ionization processes of the *manifold* states in high Rydberg states. We have measured field-ionization spectra under various conditions on the rotating electric field, and clarified their characteristic behavior. The general experimental scheme adopted

*Corresponding author. Present address: Japan Atomic Energy Research Institute, Tokai, Ibaraki 319-1195, Japan. E-mail address: yamada@neutrons.tokai.jaeri.go.jp

†Present address: Department of Physics, Osaka University, Toyonaka, Osaka 560-0043, Japan.

 ©2005 The American Physical Society

here is to start from a small electric field (of several tens of mV/cm strength, for example) in the positive z direction, and the field is decreased once to zero and then oppositely increased up to the field-ionization value (about several V/cm, for example, for the states with n around 100). In addition to this pulsed field, a static field perpendicular to the pulsed field is also applied up to a few tens of mV/cm, causing thus the rotation of the total electric field.

Specifically, in this experiment we show that the contribution of the tunneling process to the total ionization signals is strongly affected by the characteristics of the rotating electric field. Indeed, the field-ionization processes can be artificially controlled by manipulating the applied electric field shape and also the degree of field rotation. Actually the fraction of the tunneling field-ionization process can be profoundly enhanced so as to be utilized, for example, for the recently proposed stringent scheme [6] of selective field ionization in high Rydberg states.

To see how well the experimental results are reproduced with theoretical predictions, we have calculated the time evolution of the Rydberg states under rotating electric and static magnetic fields. In the theoretical treatment, we divide the whole time evolution into two regions. The first region (field-rotating regime) is at a small electric field, where the rotation of the electric field is induced and thus the redistributions of magnetic quantum number m_ℓ and parabolic quantum number n_1-n_2 of the states arise. The second region is of the following field up to field ionization, where the redistributed m_ℓ states propagate through the Stark map to reach finally the ionization field. Here depending on the m_ℓ value of the states, the populated manifold states go through adiabatic or diabatic trajectories, thus resulting in the distributions of autoionization and tunneling processes. The theoretical predictions obtained are generally in good agreement with the experimental results.

m_ℓ-changing experiments by applying electric and magnetic fields and related theoretical analysis were performed previously for several atoms with relatively low n [7–13]: These works were mainly concerned with producing a circular state, which is a state having a maximum value of $|m_\ell| = \ell = n-1$ [14]. These previous investigations are related to our present work in that both utilize the rotating field effectively. As stated before, our main aim in the present study, however, is different from theirs in that we have investigated more generally the effect of the field rotation on the field-ionization processes.

The effect of field reversal through zero crossing on the field-ionization characteristics was previously investigated by Higgs *et al.* [15] and by Rolfes *et al.* [16]. In their work, the field-rotation effect causing the m_ℓ-changing transition was not explicitly investigated.

In Sec. II the simulation scheme of our present study for the time evolution of the Rydberg states under field rotation is described. Then the setup and procedure for the present experimental study are shown in Sec. III. The experimental results and their characteristic features are presented and discussed in Sec. IV together with a detailed comparison with theoretical predictions. Finally Sec. V is devoted to the conclusion.

II. THEORY

The present simulation calculations for the time evolution of the Rydberg states are executed in two steps. The first step is a rotating-field regime where the magnitude of the pulsed field varies from its small starting value up to one much larger than the transverse static field, yet not larger than the first-crossing field value with adjacent manifold states. During this period, the rotation of the electric field is induced with a zero crossing and completed. In this regime, we mainly deal with the redistribution of the magnetic substates m_ℓ of the initial state due to the field rotation.

The second step is of the dominant pulsed-field regime where the component of the applied pulsed electric field is so large that it dominates the total electric field vector, that is, the direction of the field no longer changes greatly and thus we can safely assume that the m_ℓ value is nearly a good quantum number with the approximate cylindrical symmetry around the direction of the pulsed field. Here the transitions to different n states occur through a large number of avoided crossings. Depending on the values of m_ℓ and ℓ, each state takes its own path through the Stark map to reach the ionization stage, resulting finally in the distributions of the autoionization and the tunneling ionization events. Successive treatment of the time evolution in these two regimes gives the overall simulation process for pulsed-field ionization under a rotating electric field. We also take into account the effect of a small magnetic field of the order of the earth's field in addition to the electric field.

A. Field-rotating regime: Time evolution under a zero-crossing field rotation

Since we are here interested in the time evolution of the manifold states in the rotating-field regime, we use in good approximation the formulation by Kazansky and Ostrovsky [17] for the time evolution of hydrogen. The Hamiltonian of the valence electron of the hydrogen atom under an electric field $\mathbf{F}$ and a magnetic field $\mathbf{B}$ is given by

$$H = H_0 + \mathbf{F}(t)\cdot\mathbf{r} + \frac{1}{2}\mathbf{B}(t)\cdot\boldsymbol{\ell}, \tag{2}$$

where H_0 is the unperturbed atomic Hamiltonian, and $\mathbf{r}$ and $\boldsymbol{\ell}$ are the position vector of the electron and the orbital angular momentum, respectively. Here, we ignore the electron spin. In this Hamiltonian, we can make the replacement $\mathbf{r} \rightarrow -\frac{3}{2}n\mathbf{A}$ [17], where $\mathbf{A} = (-2H_0)^{-1/2}\left[\frac{1}{2}(\mathbf{p}\times\boldsymbol{\ell} - \boldsymbol{\ell}\times\mathbf{p}) - \mathbf{r}/r\right]$ is the Runge-Lenz vector. Introducing operators $\mathbf{I}_1 = \frac{1}{2}(\boldsymbol{\ell}+\mathbf{A})$ and $\mathbf{I}_2 = \frac{1}{2}(\boldsymbol{\ell}-\mathbf{A})$, the Hamiltonian is transformed to

$$H = H_0 + \boldsymbol{\omega}_1(t)\cdot\mathbf{I}_1 + \boldsymbol{\omega}_2(t)\cdot\mathbf{I}_2, \tag{3}$$

where

$$\boldsymbol{\omega}_1(t) = \frac{3}{2}n\mathbf{F}(t) + \frac{1}{2}\mathbf{B}(t), \tag{4}$$

$$\boldsymbol{\omega}_2(t) = -\frac{3}{2}n\mathbf{F}(t) + \frac{1}{2}\mathbf{B}(t). \tag{5}$$

The vector operators $\mathbf{I}_1$ and $\mathbf{I}_2$ have equal magnitudes, $\mathbf{I}_1^2 = \mathbf{I}_2^2 = j(j+1)$ with $j=\frac{1}{2}(n-1)$. They commute with each other and obey the commutation rule of angular momentum operators [18].

To obtain the motion of the spinlike $\mathbf{I}_k$ under the "effective" magnetic field $\boldsymbol{\omega}_k$ ($k=1, 2$), we first solve the case of the $j=1/2$ problem. By solving the time-dependent Schrödinger equation of the $j=1/2$ spin motion [17], time-propagation matrices $U^{(k)}(t,t')$ defined as $\chi_i^{(k)}(t) = U_{ij}^{(k)}(t,t')\chi_j^{(k)}(t')$ are obtained. They are represented with Euler angles $\alpha^{(k)}$, $\beta^{(k)}$, $\gamma^{(k)}$ by

$$U_{11}^{(k)}(t,t') = U_{22}^{(k)}(t,t')^* = \cos\frac{1}{2}\beta^{(k)} \exp\left(-i\frac{1}{2}(\alpha^{(k)}+\gamma^{(k)})\right),$$

$$U_{12}^{(k)}(t,t') = -U_{21}^{(k)}(t,t')^* = \sin\frac{1}{2}\beta^{(k)} \exp\left(i\frac{1}{2}(\alpha^{(k)}-\gamma^{(k)})\right). \tag{6}$$

Using the Euler angles for the case of $j=1/2$, we then obtain the time-propagation function for the case of $j\left[=\frac{1}{2}(n-1)\right]$ larger than $1/2$. For this we use the basis set $|i_1 i_2\rangle$, where i_1 and i_2 are the eigenvalues for the projections of the $\mathbf{I}_1$ and $\mathbf{I}_2$ to some fixed axes. Using the Wigner function $D^j_{mm'}(\alpha,\beta,\gamma)$ [19], the time-propagation matrix $U^{\mathrm{Ryd}}(t,t')$ is described as

$$\langle i_1 i_2|U^{\mathrm{Ryd}}(t,t')|i_1' i_2'\rangle = D^j_{i_1 i_1'}(\alpha^{(1)},\beta^{(1)},\gamma^{(1)}) \times D^j_{i_2 i_2'}(\alpha^{(2)},\beta^{(2)},\gamma^{(2)}). \tag{7}$$

If the electric field term is dominant compared to the magnetic field term in the Hamiltonian, we can assume both the magnetic quantum number m and the parabolic quantum number n_1-n_2 are good quantum numbers with the quantization axis along the electric field vector. Taking i_1 and i_2 as the projections of I_1 and I_2 to the electric field direction, respectively, they are related to m and n_1-n_2 as $m=i_1+i_2$ and $n_1-n_2=i_1-i_2$.

With the initial electric field, under which the Rydberg states are prepared, we represent the initial state as $|i_1''=[m''+(n_1''-n_2'')]/2, i_2''=[m''-(n_1''-n_2'')]/2;\mathrm{init}\rangle$. Since the initial quantization axis does not coincide with that of the final state due to the rotation of the electric field, we need to transform the initial state to a linear combination of the eigenfunctions $|i_1' i_2'\rangle$ of the final Hamiltonian:

$$|i_1'' i_2'';\mathrm{init}\rangle = \sum_{i_1' i_2'} D^j_{i_1'' i_1'}(\alpha_0,\beta_0,0) D^j_{i_2'' i_2'}(\alpha_0,\beta_0,0)|i_1' i_2'\rangle, \tag{8}$$

where α_0 and β_0 are Euler angles between the initial and final quantization axes. The population P_{m,n_1-n_2} of the final state with m and n_1-n_2 is then obtained as

$$P_{m=i_1+i_2,n_1-n_2=i_1-i_2} = \left|\sum_{i_1',i_2'} \langle i_1 i_2|U^{\mathrm{Ryd}}(t,t')|i_1' i_2'\rangle\langle i_1' i_2'|i_1'' i_2'';\mathrm{init}\rangle\right|^2. \tag{9}$$

B. Dominant pulsed-field regime: Time evolution in avoided-crossings network with a ramped electric field

Increasing further the strength of the applied pulsed field F_z, the field rotation almost ceases and the states begin to go through avoided crossings with the adjacent manifold states at $F \simeq 1/3n^5$. The states then traverse a large number of avoided crossings on the Stark map up to the ionization threshold. Here we have to take into account the quantum defects of nonhydrogenic atoms.

In the present section we describe two models to calculate the time evolution in this regime; an incoherent and a coherent model. In the incoherent multichannel Landau-Zener (MLZ) time-evolution model [20], we have performed Monte Carlo simulation calculations by neglecting the interference between the different paths in the Stark map, while in the coherent time-evolution model, we have numerically solved the Schrödinger equations including about 1000 states in which the interferences between many paths are fully taken into account.

1. Incoherent time-evolution model

In each avoided crossing, the state traverses through the diabatic or adiabatic passages. The probability P of traversing through the diabatic passage [21] is assumed to be given by the Landau-Zener model [22,23]:

$$P = \exp\left(-2\pi\frac{|\langle V_d\rangle|^2}{\hbar\dfrac{dW}{dF}\dfrac{dF}{dt}}\right), \tag{10}$$

where $\langle V_d\rangle$ is the matrix element of the interaction potential $V_d(r)$ between the crossing two levels, W is the difference in the energies of the two crossing levels, F is the applied electric field, and dF/dt is the slew rate of the applied field.

We have performed a Monte Carlo simulation calculation for the state propagation on the Stark map. The initial electric field was set to the value of 5 mV/cm, which is much less than that at the first crossing to the adjacent manifold $F \simeq 1/3n^5$. We assumed the state propagates along the hydrogen Stark map, where the energy levels are defined as

$$W_{nn_1n_2m} = -\frac{1}{2n^2} + \frac{3}{2}Fn(n_1-n_2). \tag{11}$$

When the state encounters the other levels, we randomly select the diabatic or adiabatic passage according to the probability P in Eq. (10). Here, we show the evolution of the states with $|m_\ell| \leqslant 3$ only because $|m_\ell| \geqslant 4$ states of Rb have negligibly small quantum defects so that they all propagate diabatically on the Stark map and ionize through the tunneling process like hydrogen.

The simulation results are shown in Fig. 1 for the states with $|m_\ell|=0$ to 3 at $W_r=-0.52$ in $n=112$. We use here the

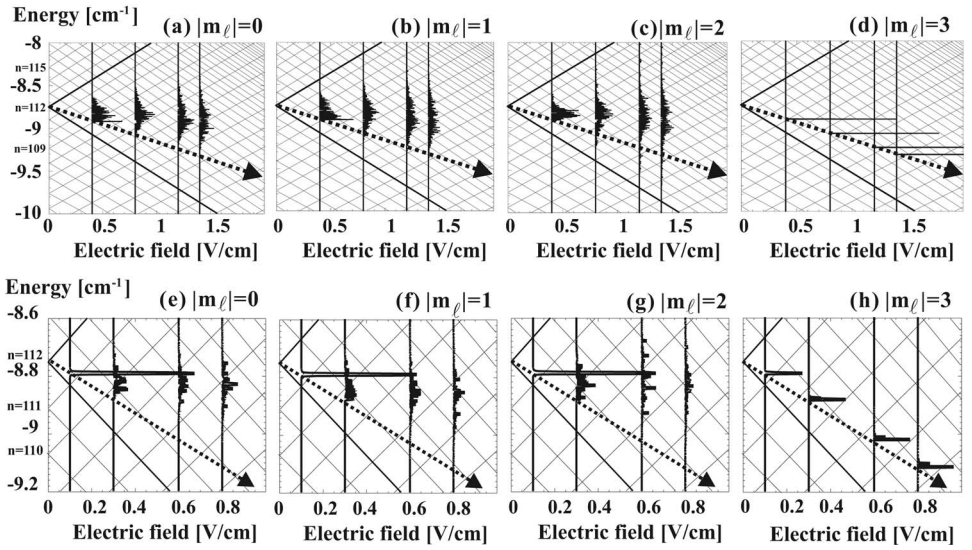

FIG. 1. Calculated results of incoherent and coherent time evolution under a ramped electric field. The results of incoherent time evolution are shown for $|m_\ell|$= (a) 0, (b) 1, (c) 2, and (d) 3. Those of coherent time evolution are shown for $|m_\ell|$= (e) 0, (f) 1, (g) 2, and (h) 3. The initial manifold state is at $W_r=-0.52$ of $n=112$ and the slew rate of the ramped electric field is 5.9 V/cm μs. Only the reddest and bluest states in each manifold are drawn in the figures to make the Stark map more transparent. Dashed arrows show the diabatic paths. In (d) and (h), the drawing scale of the magnitude for the population is reduced to five times smaller than the other cases.

variable W_r to point the position in the manifold, which is defined as $W_r=(n_1-n_2)/n$. A value of W_r close to 1 means the highest (bluest) and that close to -1 the lowest (reddest) levels in the manifold. The trial number of the Monte Carlo simulation was 1000 for each m_ℓ. As seen in Figs. 1(a)–1(c), the states with $|m_\ell|=0$, 1, and 2 propagate adiabatically, whereas the states with $|m_\ell|=3$ mostly propagate along a diabatic path shown as a dashed arrow in Fig. 1(d). This difference comes from the fact that the $|m_\ell|=3$ states mainly consist of the f component, the quantum defect of which is quite small in Rb (0.016); thus P is large enough to allow an almost diabatic path.

To obtain the fraction of the tunneling field-ionization process for each m_ℓ state, we need to know the population on the diabatic path to the tunneling ionization threshold. We have calculated the population distributions up to 1.5 V/cm with the procedure described above and then extrapolated them to the ionization threshold field of 4.35 V/cm. In this extrapolation process, we took into account the slight linear dependence of the calculated population distributions on the field strength. The populations within the region of $|\Delta n_1| \leqslant 3$, which corresponds to $|\Delta W_r| \leqslant 0.054$, was taken as the populations on the diabatic paths.

2. Coherent time-evolution model

In the coherent time-evolution model, we have numerically solved the Schrödinger equation with the following Hamiltonian where the field is ramped with the slew rate $S_z[F_z(t)=S_z t]$:

$$i\hbar \frac{d\psi}{dt} = H\psi, \tag{12}$$

$$H = \frac{1}{2}p^2 - \frac{1}{r} + S_z t z + V_d(r), \tag{13}$$

where the ℓs coupling term Λ, the static field components F_x and F_y, and the magnetic field terms were all ignored because $F_z z \gg \Lambda$, $F_x x$, $F_y y$, and $\frac{1}{2}\mathbf{B}\cdot\ell$ at this region in the dominant pulsed-field regime.

The numerical solution of Eq. (12) for the Rydberg states in Rb has been performed with a computer program developed in [24]. We have executed the calculations up to F_z =800 mV/cm ($n=112$) by including all the states within $\Delta n=5$. The total number of states included is over 1000 in each magnetic quantum number. Coherent time evolutions of an initial state at $W_r=-0.52$ in $n=112$ of Rb with $|m_\ell|$ from 0 to 3 are also shown in Fig. 1. The calculation parameters were set to the same values adopted in the present experiment; the slew rate of the electric field is 5.9 V/(cm μs). The states with $|m_\ell|=0$, 1, and 2 do not follow the diabatic path represented by a dashed arrow in the figure but rather go along the adiabatic one, where the energy of the states does not change greatly with increasing electric field. On the other hand, the $|m_\ell|=3$ states remain mainly on the diabatic path at 800 mV/cm. Note that a 20% population fraction of the $|m_\ell|=3$ states yet distributes along the path of the adiabatic line; however, they are not clearly seen in the figure because of their rather wide distributions. In order to obtain the population on the diabatic path at the ionization threshold field for the tunneling process, we have adopted the same extrapolation procedure as in the case of incoherent model calculations.

Related to the above theoretical predictions, we note here that recently Førre and Hansen [25] calculated the time evolution of a lithium Rydberg state with n of 25 in a Stark map with both a quantal coherent and an incoherent MLZ model,

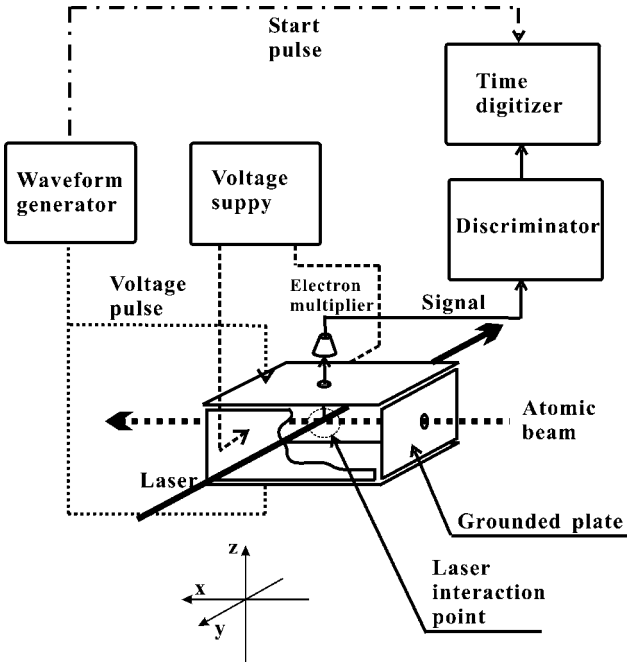

FIG. 2. Schematic view of the present experimental setup. The coordinate system used in this paper is also shown.

and their simulation results were compared with each other. They obtained nearly equivalent results in the coherent and incoherent model calculations for the population probabilities of states passing through the adiabatic and diabatic paths in the Stark map. Their results and conclusions are generally consistent with our present results of the theoretical treatment, although our present case is a more complicated situation due to the profound number of involved states.

III. EXPERIMENTAL SETUP AND PROCEDURE

A schematic diagram of the present experimental setup is shown in Fig. 2. A thermal atomic beam of ^{85}Rb from an oven at 110 °C is introduced to the region surrounded by six copper plates. The ground-state atoms are excited to a Rydberg state by a two-step process. As the first step, a diode laser (Sharp GH0780MA2C) was used to excite the atoms in the beam from the ground state ($5s_{1/2}$) to the $5p_{3/2}$ excited state. As the second step, a ring dye laser (Coherent 899-29) pumped by a Kr-ion laser was used to excite the atoms in the $5p_{3/2}$ state to the final Rydberg state. The excitation spectra are shown in Fig. 3. To know the absolute wavelength of the second ring dye laser, the absorption spectrum of tellurium molecules was also measured [26].

The adopted polarization of the diode and the dye lasers is perpendicular and parallel to the applied electric field, respectively. The states with $|m_J|=1/2$ or $3/2$ are therefore allowed as the final Rydberg states by the selection rule and the states have components of $|m_\ell|$ from 0 to 2.

The region for the excitation and ionization of the Rydberg atoms is surrounded by six copper plates. The top and bottom electrodes are used to apply the pulsed electric field for the field ionization. The electrodes are of area 210

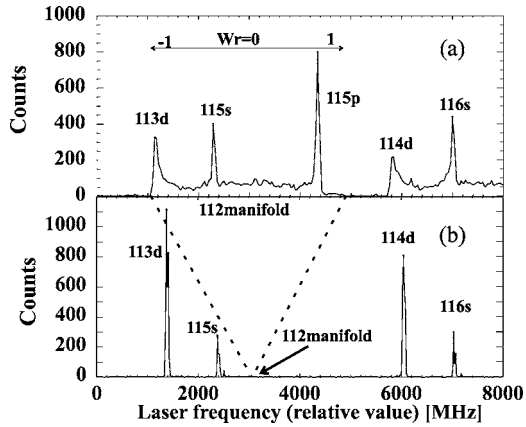

FIG. 3. Typical excitation spectra of the $n=112$ manifold states of ^{85}Rb (a) with the applied electric field of 80 mV/cm, and (b) without field.

$\times 210$ mm^2 and the gap between them is 60 mm. The top electrode has a hole of 5 mm diameter, through which ionized electrons are collected by an electron multiplier. The two side electrodes are for generating a static field perpendicular to the pulsed field. The rest of the electrodes are grounded.

A voltage pulse is produced by a wave-form generator (Sony Tektronix AWG420) to apply to the ionization electrodes. The field was typically changed from 20 mV/cm to −6 V/cm within 0.25–4 μs in the present experiment. The precise determination of the slew rate of the field was done by measuring the wave form with a digital oscilloscope.

Ionized electrons were collected by a channel electron multiplier. Output signals of the multiplier are amplified by a preamplifier and then by two main amplifiers. The signals are then fed to a discriminator and counted by a multiple-event time digitizer (Fast Comtec P7886), which records the interval between a start signal generated from the wave-form generator and the signal from the discriminator.

IV. EXPERIMENTAL RESULTS AND DISCUSSION

In addition to the applied fields, there exists a stray electric field produced by the surroundings such as surface contamination of electrodes. Here, we define $\mathbf{F}^{\text{total}}$ as the total field that the Rydberg atoms experience:

$$\mathbf{F}^{\text{total}} = \mathbf{F}^{\text{app}} + \mathbf{F}^{\text{stray}}, \tag{14}$$

where $\mathbf{F}^{\text{app}}$ is the applied field by the four electrodes, and $\mathbf{F}^{\text{stray}}$ is the stray field. We also define $\mathbf{F}^{\text{cal}}$ as the field in the simulation and we will use $\mathbf{F}$ as both $\mathbf{F}^{\text{total}}$ and $\mathbf{F}^{\text{cal}}$.

Before data taking, special care was taken to reduce the stray field. In the present experiment its absolute value was measured to be 4.7 mV/cm. The z component F_z^{stray} has little influence on the condition of the experiment, because the pulsed field with zero crossing can cancel it. The value of F_y^{stray} was determined to be about 1.3 mV/cm from the measurement as described in the next subsection. Therefore, only the value of the x component of F_x^{stray} remains unknown, which should be less than 4.7 mV/cm from the known absolute value.

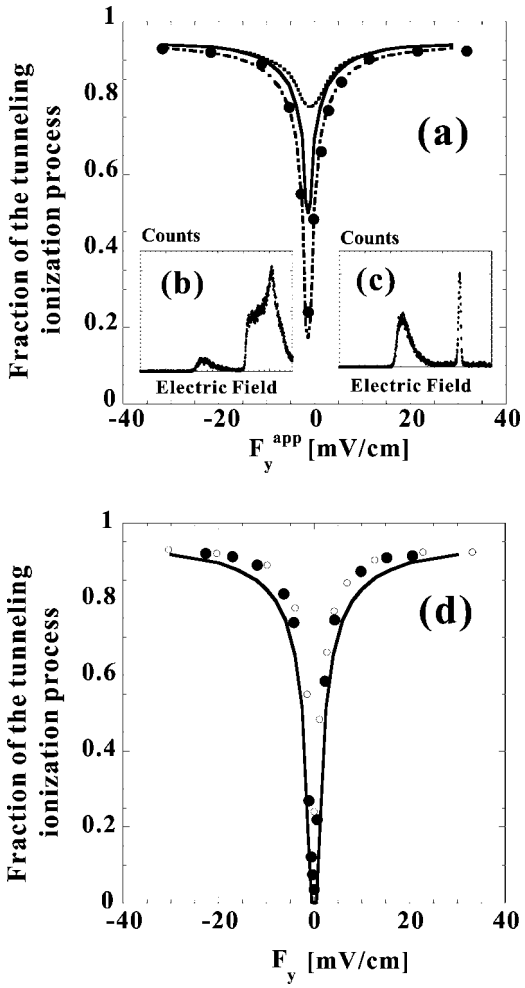

FIG. 4. Dependence of the fraction of the tunneling field-ionization process on the transverse electric field F_y^{app}. The initial value of W_r is 0.30 with a quantization axis along the direction of the initial electric field, and the slew rate F_z adopted is 5.9 V/cm μs. (a) Solid circles show the experimental data and the three lines are calculated results with the following values of F_x^{cal} and magnetic field: F_x^{cal} and $|\mathbf{B}|/|\mathbf{B}^{\mathrm{geo}}|$ 0 mV/cm and 1/2 (dash-dotted line), 0 mV/cm and 1.0 (solid line), and 5 mV/cm and 1.0 (dotted line), respectively. Taking into account the existence of the stray field of 1.3 mV/cm strength in the y direction, the calculated lines are shifted by $\Delta F_y^{\mathrm{cal}}=-1.3$ mV/cm such that the minimum of the calculated fraction matches that of the experimental one. In the inset are shown typical ionization spectra at F_y^{app}= (b) −21.7 and (c) −1.3 mV/cm. (d) Solid and open circles show the experimental data with and without the geomagnetic field canceled out, respectively. Solid line is a theoretical prediction without the external magnetic field. Assumed values of F_x^{cal} and magnetic field adopted: F_x^{cal} and $|\mathbf{B}|/|\mathbf{B}^{\mathrm{geo}}|$ 0 mV/cm and 1/2 (dash-dotted line), 0 mV/cm and 1.0 (solid line), and 5 mV/cm and 1.0 (dotted line), respectively. For simplicity, the effect of the stray electric field was included in the values of the transverse electric field of the abscissa so that the ionization fraction takes a minimum at zero transverse electric field F_y^{app}.

In the present experimental situation, states with $|m_\ell|$ of 0 to 2 can only be populated by laser excitation from the $5p_{3/2}$ state. The effect of the different contributions from each m_ℓ state is considered to be small because the redistribution effect of m_ℓ due to the field rotation is much larger. For the same reason, the effect of the mixing due to ℓs coupling is insignificant in the present situation.

A. Transverse-field dependence of the fraction of the tunneling field ionization

We have measured field-ionization spectra under a rotating electric field with various transverse fields F_y^{app}. The pulsed electric field F_z^{app} was ramped from 80 mV/cm to about −6 V/cm. In Fig. 4(a) is shown the dependence of the tunneling field-ionization fraction on the value of F_y^{app}. In the inset typical ionization spectra at two F_y^{app} values are shown. The data were obtained with the geomagnetic field in addition to the applied electric field. The fraction of the tunneling field ionization increases rapidly over 90% with increasing $|F_y^{\mathrm{app}}|$, which clearly indicates m_ℓ redistributions by the field rotation.

It is noted here that the measured fraction of the tunneling field-ionization process takes the minimum value at $F_y^{\mathrm{app}}=-1.3$ mV/cm. This deviation from zero of the value of F_y^{app} at minimum is considered to be due to the effect of a stray field along the direction of the y axis, that is, $F_y^{\mathrm{stray}}=1.3$ mV/cm. The three lines in the figure represent the calculated results with various values of the field F_x^{cal} and magnetic field $\mathbf{B}^{\mathrm{cal}}$. As the values of these parameters become smaller, the calculated dip becomes deeper.

The above result shows that about 20% fraction still remains in the tunneling field-ionization process even without the transverse electric field. This contribution is due to the existence of the geomagnetic field: Fig. 4(b) shows the dependence of the tunneling field-ionization fraction on the value of F_y^{app} with the geomagnetic field canceled out. The geomagnetic field was canceled out by conducting currents into three-axis Helmholtz coils around the experimental area. The magnetic field was thus reduced to less than 2 μT. The tunneling ionization fraction is almost zero at the zero transverse electric field. In the figure theoretical predictions are also shown together with the experimental results with the geomagnetic field for comparison. The theoretical predictions reproduce well the experimental results. Taking into account a small unknown value of the stray electric field in the x direction, simulation results are thus generally in good agreement with the experimental results for both the cases of the external magnetic field canceled (b) and not canceled (a).

B. Slew rate and principal-quantum-number dependence

In Fig. 5 is shown the dependence of the fraction of the tunneling field-ionization process on the slew rate. The theoretical results show a slight decrease with increasing slew rate, the tendency of which is in good agreement with the experimental results. This tendency is due to the fact that the m_ℓ-changing effect of the rotating electric field is weaker with increasing slew rate of the applied pulsed field; thus the resulting states tend to remain more at the same initial low-m_ℓ states. Since the low-m_ℓ states ionize more through the autoionizationlike process, the tunneling fraction thereby decreases with increasing slew rate.

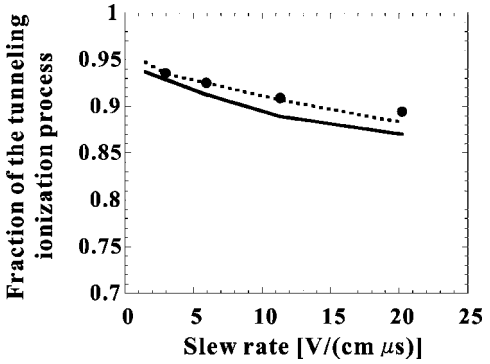

FIG. 5. Slew-rate dependence of the fraction of the tunneling field-ionization process for the initial $n=112$ manifold state of ^{85}Rb. Solid circles show the experimental results. Two lines are the calculated results where F_x^{cal} and $|\mathbf{B}|/|\mathbf{B}^{\mathrm{geo}}|$ are 0 mV/cm and 1/2 (solid line), and 5 mV/cm and 1.0 (dotted line), respectively. The initial value of W_r is 0.52 and $F_y=-21.3$ mV/cm.

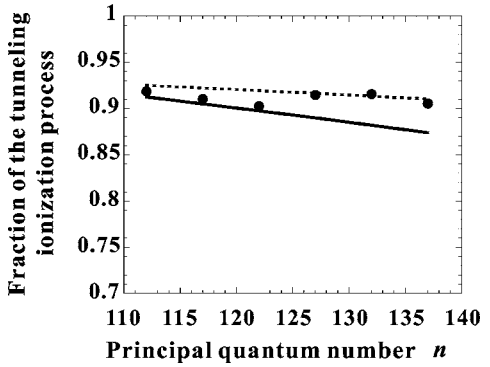

FIG. 6. Principal-quantum-number n dependence of the fraction of the tunneling field-ionization process. Solid circles show the experimental results. Two lines show calculated results: F_x^{cal} and $|\mathbf{B}|/|\mathbf{B}^{\mathrm{geo}}|$ are 0 mV/cm and 1/2 (solid line), and 5 mV/cm and 1.0 (dotted line), respectively. The initial value of W_r is 0.52. The slew rate of the applied pulsed electric field F_z is 5.9 V/cm μs. The values of F_y applied for the six n data points are −21.6, −17.7, −14.6, −11.7, −9.2, and −7.8 mV/cm, respectively, from lowest to highest n.

The dependence of the tunneling field-ionization fraction on the principal quantum number n has been also measured, which is shown in Fig. 6. The fraction observed experimentally almost does not depend on the number n, although the calculated value decreases slightly with increasing n.

V. CONCLUSION

We have investigated both experimentally and theoretically the effect of the rotating electric field on the field-ionization processes in the highly excited ^{85}Rb Rydberg manifold states at $112 \leqslant n \leqslant 137$. Specifically we have measured field-ionization spectra under the rotating electric field by applying a longitudinal pulsed electric field together with a variable transverse static field. The field rotation near the zero-crossing region was found to bring an increase of the fraction of the tunneling field-ionization process and also the broadening of the tunneling field-ionization peak. These effects almost do not depend on the slew rate of the applied pulsed field, and also on the principal quantum number n from 112 to 137.

In order to compare these experimental results with theoretical predictions, we have calculated the time evolution of the Rydberg state under a rotating electric field. The simulation consists of calculating the m_ℓ and n_1-n_2 redistributions under a rotating electric field as the first step and then of tracing the propagation of each m_ℓ state on the Stark energy diagram as the final step. In the final step, we performed both fully quantal coherent calculations and multichannel Landau-Zener incoherent calculations. The theoretical results are generally in good agreement with the experimental results, indicating clearly that these effects are due to m_ℓ and n_1-n_2 redistributions under a rotating electric field. The effect of a small magnetic field on the order of the geomagnetic one together with a rotating electric field was also investigated both experimentally and theoretically, revealing its important role also in the redistributions of the m_ℓ and n_1-n_2 states.

These comparisons also indicate that the experimental results for the time evolution of manifold states in Rb are well explained by observations that the states with $|m_\ell| \leqslant 2$ and a small amount of the state of $|m_\ell|=3$ traverse the avoided crossings adiabatically, while the states with $|m_\ell| \geqslant 3$ mostly pass the crossings diabatically for the range of the slew rate adopted in the present study (from 1.5 to 20.2 V/cm μs). The states passing through the adiabatic trajectory are then ionized with an autoionizationlike process, whereas the states going through the diabatic path are ionized with the hydrogenic tunneling field-ionization process.

The present results for the effect of the rotating electric field on the field-ionization processes provide essential information on the basis of the recently proposed stringent scheme [6] for selective field ionization: Strong enhancement of the tunneling field-ionization process with a properly adopted rotating electric field through zero crossings improves appreciably the efficiency of this detection scheme.

ACKNOWLEDGMENT

This research was partly supported by a Grant-in-aid for Specially Promoted Research (Grant No. 09102010) by the Ministry of Education, Culture, Sports, Science and Technology, Japan.

[1] M. G. Littman, M. M. Kash, and D. Kleppner, Phys. Rev. Lett. **41**, 103 (1978).
[2] T. H. Jeys, G. W. Foltz, K. A. Smith, E. J. Beiting, F. G. Kellert, F. B. Dunning, and R. F. Stebbings, Phys. Rev. Lett. **44**, 390 (1980).
[3] *Rydberg States of Atoms and Molecules*, edited by R. F. Stebbings and F. B. Dunning (Cambridge University Press, Cambridge, U.K., 1983).
[4] T. F. Gallagher, *Rydberg Atoms* (Cambridge University Press, Cambridge, U.K., 1994), and references cited therein.
[5] Y. Kishimoto, M. Tada, K. Kominato, M. Shibata, S. Yamada, T. Haseyama, I. Ogawa, H. Funahashi, K. Yamamoto, and S. Matsuki, Phys. Lett. A **303**, 279 (2002).
[6] M. Tada, Y. Kishimoto, M. Shibata, K. Kominato, S. Yamada, T. Haseyama, I. Ogawa, H. Funahashi, K. Yamamoto, and S. Matsuki, Phys. Lett. A **303**, 285 (2002).
[7] D. Richards, J. Phys. B **17**, 1221 (1984).
[8] M. Gross and J. Liang, Phys. Rev. Lett. **57**, 3160 (1986).
[9] J. C. Day, T. Ehrenreich, S. B. Hansen, E. Horsdal-Pedersen, K. S. Mogensen, and K. Taulbjerg, Phys. Rev. Lett. **72**, 1612 (1994).
[10] K. S. Mogensen, J. C. Day, T. Ehrenreich, E. H. Pedersen, and K. Taulbjerg, Phys. Rev. A **51**, 4038 (1995).
[11] L. Kristensen, E. Horsdal-Pedersen, and P. Sørensen, J. Phys. B **31**, 1049 (1998).
[12] R. Lutwak, J. Holley, P. P. Chang, S. Paine, D. Kleppner, and T. Ducas, Phys. Rev. A **56**, 1443 (1997).
[13] J. Hare, M. Gross, and P. Goy, Phys. Rev. Lett. **61**, 1938 (1988).
[14] R. G. Hulet and D. Kleppner, Phys. Rev. Lett. **51**, 1430 (1983).
[15] C. Higgs, M. A. Fineman, F. B. Dunning, and R. F. Stebbings, J. Phys. B **15**, L697 (1982).
[16] R. G. Rolfes, D. B. Smith, and K. B. MacAdam, J. Phys. B **16**, L533 (1983).
[17] A. K. Kazansky and V. N. Ostrovsky, J. Phys. B **29**, L855 (1996).
[18] W. Pauli, Z. Phys. **36**, 336 (1926).
[19] L. D. Landau and E. M. Lifshitz, *Quantum Mechanics: Non-Relativistic Theory* (Pergamon, New York, 1977).
[20] D. A. Harmin and P. N. Price, Phys. Rev. A **49**, 1933 (1994).
[21] J. R. Rubbmark, M. M. Kash, M. G. Littman, and D. Kleppner, Phys. Rev. A **23**, 3107 (1981).
[22] L. D. Landau, Phys. Z. Sowjetunion **2**, 46 (1932).
[23] C. Zener, Proc. R. Soc. London, Ser. A **137**, 696 (1932).
[24] Y. Kishimoto, Mem. Fac. Sci., Kyoto Univ., Ser. Phys., Astrophys., Geophys. Chem **38**, 163 (2002); S. Yamada, *ibid.* **45**, 47 (2004).
[25] M. Førre and J. P. Hansen, Phys. Rev. A **67**, 053402 (2003), see also F. Robicheaux and C. Wesdorp and L. D. Noordam, *ibid.* **62**,043404 (2000).
[26] T. Haseyama *et al.*, Phys. Lett. A **317**, 450 (2003).